Title:

Combined geophysical measurements provide evidence for unfrozen water in permafrost in the Adventdalen valley in Svalbard

In preparation for: *Geophysical Research Letters*

Revised version submitted 29 March 2018

Authors:

Kristina Keating[1], Andrew Binley[2], Victor Bense[3], Remke L. Van Dam[4,5], Hanne H. Christiansen[6]

[1] Department of Earth and Environmental Science, Rutgers University – Newark, 101 Warren Street, Smith Hall Room 135, Newark, NJ 07102, USA
[2]Lancaster Environment Centre, Lancaster University, Lancaster, LA1 4YQ, UK
[3]Department of Environmental Sciences, Wageningen University, PO Box 47, 6700AA Wageningen, Netherlands
[4] Department of Civil Engineering, Centro Federal de Educação Tecnológica de Minas Gerais (CEFET-MG), CEP 30510-000, Belo Horizonte, Brazil
[5] Department of Earth and Environmental Sciences, Michigan State University, East Lansing, MI 48824, USA
[6]Arctic Geology Department, The University Centre in Svalbard, P.O. Box 156, 9171 Longyearbyen, Norway

Key Points:

- Surface nuclear magnetic resonance and controlled source audio-magnetotelluric measurements used to map permafrost in Adventdalen, Svalbard
- Measurements provided direct *in situ* detection of unfrozen water in permafrost
- Up to 10% unfrozen water content was detected using surface nuclear magnetic resonance in measurements made below the marine limit

Index terms (up to 5): 0702 Permafrost, 0794 Instruments and techniques, 0925 Magnetic and electrical methods (5109)

Key words: arctic, coastal, permafrost, Svalbard, SNMR, CSAMT

Abstract

Quantifying the unfrozen water content of permafrost is critical for assessing impacts of surface warming on the reactivation of groundwater flow and release of greenhouse gasses from degrading permafrost. Unfrozen water content was determined along a ~12 km transect in the Adventdalen valley in Svalbard, an area with continuous permafrost, using surface nuclear magnetic resonance and controlled source audio-magnetotelluric data. This combination of measurements allowed for differentiation of saline from fresh, and frozen from unfrozen pore water. Above the limit of Holocene marine transgression no unfrozen water was detected, associated with high electrical resistivity. Below the marine limit, within several kilometers of the coast, up to ~10% unfrozen water content was detected, associated with low resistivity values indicating saline pore water. These results provide evidence for unfrozen water within continuous, thick permafrost in coastal settings, which has implications for groundwater flow and greenhouse gas release in similar Arctic environments.

1 Introduction

It is often assumed that permafrost, defined as any Earth material that remains below 0ºC for two consecutive years (French, 2007), indicates that the pore water is frozen. However, permafrost in sediments may have a substantial unfrozen water content, for instance in coastal environments with saline intrusion, when the sediment and original pore fluids are littoral or marine in origin, or in warm permafrost, i.e., permafrost at or just below 0ºC (e.g., Overduin et al., 2012; Romanovsky & Osterkamp, 2000). While frozen ground is considered an impermeable barrier for groundwater movement, partially frozen ground may allow for considerable flow, which has significant implications for heat and mass transport processes (e.g., Bense et al., 2009; Boike et al., 1998; Romanovsky & Osterkamp, 2000; Walvoord & Kurylyk, 2016). As such, understanding the ice/water content of permafrost is critical for modelling permafrost evolution and predicting the effect of climate change on the degradation of permafrost and consequent impact on the carbon cycle and groundwater-surface water exchange processes (Bense et al., 2012).

Currently, there is a lack of data documenting the unfrozen hydrogeologic characteristics of permafrost, which severely limits the potential to accurately model hydrologic processes in permafrost landscapes (Walvoord & Kurylyk, 2016). The thickness and location of permafrost is typically determined from measurements of temperature or by modelling, which do not directly relate to the unfrozen water content. Furthermore, in warm permafrost the unfrozen water content can be substantial, up to ~20% of the total porosity for soils at -1ºC depending on the soil and pore-fluid composition (Romanovsky & Osterkamp, 2000). Cores collected from permafrost environments are typically moved to freezers held at e.g. -12ºC prior to analysis (Gilbert, 2014). This may cause components of the core that were unfrozen at *in situ* conditions to freeze prior to analysis making it difficult to quantify the unfrozen water content in the laboratory. In contrast, geophysical measurements made in a borehole can provide *in situ* information about the physical state of pore water (e.g., Kass et al., 2017; Minsley et al., 2016; Romanovsky & Osterkamp, 2000). Such measurements can provide the unfrozen water content; however, the data are limited to borehole locations. To provide data for larger scale permafrost models, more spatial information is needed.

Surface-based geophysical measurements can be used to characterize the depth and distribution of permafrost; an overview of large scale permafrost mapping can be found in (Walvoord & Kurylyk, 2016). Geophysical investigations have primarily consisted of electrical and electromagnetic measurements in environments where permafrost is assumed to be frozen, including in mountainous and high-latitude settings. In these environments, permafrost has a high resistivity (>~1000 Ωm in the absence of clay) and unfrozen ground has low resistivity (<~500 Ωm; Minsley et al., 2012). Examples include airborne electromagnetic measurements (e.g., Minsley et al., 2012), direct current resistivity (e.g., Hilbich et al., 2008; Hubbard et al., 2013), and magnetotellurics (e.g., Koziar & Strangway, 1978). In coastal environments and with groundwater brines, the interpretation of electrical resistivity data becomes more complex as both frozen and unfrozen sediments can have low resistivity, e.g. < 200 Ωm as observed by Mikucki et al. (2015) in the McMurdo Dry Valleys in Antarctica, Overduin et al. (2012) in Alaska, and by Ross et al. (2007) in the Adventdalen valley, Svalbard. This makes it difficult to use electrical resistivity measurements alone to understand the physical state of pore water as either frozen, partially frozen, or liquid.

Surface nuclear magnetic resonance (SNMR), which is sensitive to unfrozen water content, is emerging as a geophysical method that, alongside electrical resistivity measurements, can be used to investigate permafrost environments (Behroozmand et al., 2015; Parsekian et al., 2013). Due to the impact of the subsurface electrical resistivity structure on the SNMR signal, electrical or electromagnetic geophysical measurements are typically collected together with SNMR measurements (Behroozmand et al., 2015). Previous studies have successfully demonstrated the use of SNMR to determine the thickness of taliks, a layer or body of unfrozen ground that occurs in permafrost, and to determine the depth of permafrost (Parsekian et al., 2013).

In this study, we used controlled source audio magnetotelluric (CSAMT) and SNMR measurements to map the physical state of permafrost and distinguish frozen from unfrozen water in the permafrost in the Adventdalen valley in Svalbard at 78°N. The SNMR measurements were used to determine the unfrozen water content, whereas the CSAMT measurements, which are sensitive to changes in the electrical resistivity, were used in the inversion of the SNMR measurements, and to distinguish saline from fresh pore water and frozen from unfrozen ground. To the best of the authors' knowledge, this study is the first to successfully employ CSAMT and SNMR to detect unfrozen water content within continuous permafrost.

2 Site description

Field data were collected in the Adventdalen valley (hereafter only called Adventdalen) in Svalbard at 78°N. This flat-bottomed river valley is partly infilled with Holocene marine, deltaic, fluvial and periglacial sediments, in a typical coastal Arctic high relief landscape with continuous permafrost of -3˚C to -6˚C at 10 m depth (Christiansen et al., 2010; Gilbert, 2018) (Figures 1 and 2). Typically, the upper 3-4 m of sediment is aeolian with a relatively high amount of syngenetic ground ice in the permafrost, all of which accumulated since 3 ka ago in the middle of Adventdalen, after the underlying deltaic sediments became subaerially exposed (Gilbert, 2018). Sediments below this depth are primarily deltaic with epigenetic permafrost and a generally low ground ice content (Gilbert, 2018). The upper deltaic sediments consist of approximately even amounts of silt and sand, with less than 5% clay, and were deposited in delta top and delta front facies assemblages. The deepest studied sediments in one core below 35 m are finer-grained with up to 10% clay and around 15 % sand; deposited in glaciomarine and prodelta environments (Gilbert, 2014, 2018). Raised marine deposits, indicating the upper Holocene marine limit, in Adventdalen, dated to ~10 ka, occur at 70 m a.s.l. in its outer part and at 62 m a.s.l. in the inner part (Lønne & Nemec, 2004; Lønne, 2005). Adventdalen features typical periglacial landforms including pingos and ice-wedges. Thermal profiles from borehole records show that in Adventdalen the permafrost is typically 80 to 100 m thick, and is assumed to thin to 0 m at the shore. In the mountains surrounding the valleys the permafrost can reach a thickness of 400 m (Humlum, 2005; Svensson, 1970). The active layer in Adventdalen is ~1m thick (Figure 2; Christiansen, 2005).

The average gravimetric ice content, determined in a 60 m continuous core extracted from the UNIS-CO_2 borehole (Figure 1) and placed directly in a -12 ˚C freezer, generally ranges from 20 to 40% (Gilbert, 2018). However, the near surface terrestrial sediments (from depths < 5m) can have gravimetric ice contents up to 160%, due to the presence of ice-wedges and/or the formation of syngenetic permafrost in the terrestrial sediments (Gilbert, 2018).

3 Geophysical methods

SNMR and CSAMT measurements were collected both along and across Adventdalen (Figure 1) from 23 March to 2 April 2013. During this time, the ground was snow covered, the active layer was frozen (Figure 2), and the valley was accessible by snow mobile enabling effective surveys across the entire valley bottom.

CSAMT measurements were collected at 13 locations using a Geometrics Stratagem EH4 system with a frequency range from 11.7 Hz to 100 kHz. Information at depth was obtained by recording data from natural signals; information from shallow depths was obtained by recording data from a high frequency 400 Am^2 controlled source several hundred meters from the receiver. The electrodes were arranged with 40 m spacing. To ensure good electrical contact with the ground, electrode sites were predrilled to approximately 20cm and a saline solution was poured over the electrodes prior to the collection of each CSAMT dataset and supplemented as needed during the data collection. The CSAMT data were inverted using IPI2win (Bobachev, 2002) to create a blocky 1D model at each receiver station. Datasets with high noise (due to problems with maintaining electrode contact in frozen ground) were discarded.

SNMR measurements, which are directly sensitive to hydrogen protons in water, were collected at 15 locations using a 70x70 m square loop with the Vista Clara GMR system. Although in theory SNMR measurements are sensitive to hydrogen in both ice and unfrozen water (Kleinberg & Griffin, 2005), the fast relaxation time of ice means that it cannot be detected using NMR equipment with long “deadtimes”, i.e., time between the excitation pulse and the first data point, such as in SNMR instruments. The remote location meant that the anthropogenic noise was limited to snow mobiles and a 50 Hz power line located along the road indicated in Figure 1. When possible, the snow mobile engines were turned off during the SNMR data collection and SNMR measurements were made away from the power line. Between 16 and 20 stacks were collected at each location. The pulse duration was set to 40 ms resulting in a maximum pulse moment of 14.19 A·s.

To account for variations in the magnetic field, its strength was measured using a proton precession magnetometer during the SNMR measurements. In Adventdalen the magnetic field declination is 7.5º and the inclination is 82º. The total magnetic field strength varied from 54 674 nT to 54 819 nT across all measurement locations; the maximum variation during a single measurement was 130 nT (for site SNMR04), while the average variation during individual measurements was 41 nT. The Larmor frequency, f_0, is calculated from the magnitude of Earth's magnetic field, B_E, using $f_0 = \gamma_H B_E / 2\pi$, where γ_H is the gyromagnetic ratio for protons in water ($\gamma_H / 2\pi$ = 42.577 MHz/T). The SNMR excitation pulse is tuned to the Larmor frequency, which allows for the selective excitation of hydrogen protons. The variation in the Larmor frequency during the course of a single measurement ranged from 0.2 to 2.3 Hz for most SNMR profiles, but was higher for SNMR03 (3.7 Hz) and SNMR04 (5.5 Hz); this variation is within the acceptable range of frequency offsets for accurate inversion of SNMR data (Walbrecker et al., 2011).

The SNMR data were first processed using the GMR processing software (Walsh, 2008) and filtered with a 100 Hz bandpass filter. Individual records with high noise levels (primarily due to snow mobiles) were removed prior to stacking the datasets. The filtered and stacked SNMR datasets were inverted using an open-source NMR processing package (MRSMATLAB; Müller-Petke et al., 2012). This package uses a QT inversion scheme, which simultaneously fits all pulse moments, signal amplitudes, and relaxation times, to determine the water content and relaxation time profiles (Müller-Petke and Yaramanci, 2010). The data were fit assuming that relaxation started following the applied pulse, i.e., not accounting for relaxation during pulse (RDP); this approach was used because, for signals with short relaxation times (< the length of the applied pulse), accounting for RDP can result in over- or under-estimation of the total water content (Grombacher et al., 2017; Walbrecker et al., 2009). Four-layer blocky inversion models were used for all data sets. Uncertainty is shown by displaying models that fit the data approximately equally well as the best fit, i.e., have a similar chi-squared statistic; 6 to 12 equivalent models are shown for each profile. When possible, the SNMR data were inverted using the resistivity structure determined from a collocated CSAMT measurement; when there was no collocated CSAMT measurement at the SNMR location, the resistivity structure determined from the nearest noise-free CSAMT measurement was used.

4 Results

Results from the SNMR and CSAMT measurements are shown for the down-valley profile in Figure 3 and the two across-valley profiles in Figure 4. The inverted resistivity images show a trend towards higher resistivity at the top of the valley. Near the coast the resistivity is low, reaching a minimum of ~1 Ωm. A number of inversions of the CSAMT data show vertical profiles with significant contrasts in resistivity, some with thin low resistive layers, e.g. CSAMT13. These profiles represent a best fit to the data but, as in all inverse models, alternative models with near equivalent misfit exist. Using CSAMT13 as an example, the best fit model (RMS misfit 9.7%) contains a 1Ωm layer between 9.4m and 12.2m, however, using the equivalence modeling option in IPI2win a minimum resistivity of 0.7Ωm between 10.1 and 12.2m and a maximum resistivity of 5.1Ωm between 4.4m and 21.4m are computed (with RMS misfits of 10.6% and 11.7%, respectively). Despite such variation in near equivalent models the data confirm the presence of a shallow low resistivity layer, which we attribute to the presence of unfrozen saline pore water.

The depth of investigation for the SNMR measurements, shown as a red line in each inverted SNMR plot in Figures 3 and 4, is much shallower than typically expected for measurements collected with a 70 m square loop, < 50 m below the surface in some locations. The shallow depth of investigation is likely due to the low resistivity of the sediment near the coast, and the high magnetic field inclination (Berhoozmand et al., 2015; Hertrich, 2008). In Figures 3 and 4, the uncertainty associated with the inversion is shown by displaying models (as thin grey lines) that fit the data approximately as well as the model of best fit.

Substantial variation can be seen in the water content in the down-valley profile. Near the coast, a clear signal from unfrozen water was observed in the SNMR data, with maximum unfrozen water contents ranging from 2 to 10% in each sounding. In SNMR12, SNMR10, SNMR11 and SNMR08, the peak water content is in a single layer in the top 20 m below the surface. No unfrozen water content was detected in the SNMR measurements collected near the upper Holocene marine limit at ~62 m a.s.l. (Lønne & Nemec, 2004; SNMR06 and SNMR07 in Figure 3). The base of the permafrost, which would be indicated by higher unfrozen water content at depth, was not observed in any of the SNMR datasets, as the measurements did not penetrate below 80 m in the lower valley bottom. The relaxation times associated with the unfrozen water content in the down-valley profile were short and ranged from 8 to 50 ms.

Less variation is seen in the across-valley profiles. In the across-valley profile 1, located closer to the coast, all profiles show a maximum unfrozen water content between 3.5 and 10%, with the exception of SNMR02, which was located on the northern side of Adventdalen and shows no unfrozen water content. The resistivity sounding (CSAMT04) at the northern side of the profile also indicates a more resistive subsurface in comparison to the valley center. The modeled resistivities at CSAMT04 are, however, less than 30 Ωm, which may be attributed to silt/clay contributions. For the across-valley profile 2, which is located further up the valley, less unfrozen water was detected and little variation is seen across the valley (between 1.5 and 6%). Again, the base of the permafrost was not observed in any of the SNMR datasets. As with the mean log relaxation times in the down-valley profile, the mean log relaxation times associated with the unfrozen water content in the across-valley profiles were short and ranged from 8 to 47 ms for across-valley profile 1 and from 11 to 42 ms for across-valley profile 2.

5 Discussion

Based on the temperature profiles collected in the boreholes in Adventdalen (Figure 2), it would be assumed that the pore water within the permafrost is frozen; however, the SNMR results show that the permafrost near the coast contains unfrozen water. The SNMR profiles suggest that the unfrozen water content is as high as 10%. The low resistivity values associated with the unfrozen water content further suggests that the pore water is saline, depressing the freezing point of the pore water. The SNMR results shown were collected sufficiently far from the power lines and contain very little noise (SNMR 13 was collected near the power lines and had high noise levels, but was not used in our interpretation), and we can thus be confident in our findings. We note, however, that the exact shape of the unfrozen water content profiles (Figures 3 & 4) is affected by the inversion approach and thus some features, such as the thickness of the layer of higher water content in SNMR03, cannot be determined exactly, as indicated by the models showing uncertainty.

Furthermore, we note that SNMR inversions are strongly affected by the subsurface resistivity structure. The threshold for when the subsurface resistivity affects the SNMR inversion is a function of loop size; when the resistivity falls below this threshold, i.e., 70 Ωm for this study, it will impact the SNMR inversion (Braun & Yaramanci, 2008). Thus, for the SNMR data collected near the coast with low resistivity value, errors in the resistivity structure can impact the resulting SNMR profile. If the true resistivity is lower than determined here, then the SNMR profile would have a shallower depth of investigation and a larger maximum water content. Similarly, if the true resistivity is higher than determined here, then the SNMR profile would have deeper depth of investigation and a smaller maximum water content. Examples demonstrating the potential effect of errors in the resistivity structure are shown in Figure S1 for SNMR profiles SNMR03 and SNMR12.

Additionally, the unfrozen water content profiles provide a generalized overview of the subsurface that does not capture the complexity associated with small-scale periglacial subsurface landforms such as ice layers (Gilbert, 2018) and ice-wedges. However, the results shown here do provide a conceptual overview of the patterns and distribution of the unfrozen water content in Adventdalen, at the scale of a coastal valley in a typical Arctic setting.

The relatively shallow depth of investigation observed in the SNMR measurements (< 50 m below the surface in some locations), will limit future use of SNMR to image the permafrost base in Adventdalen. In a typical survey the pulse length (to a maximum of 40 ms, the pulse length used in this study) and loop size can be enlarged to increase the depth of investigations. We thus recommend that in future applications of SNMR in Adventdalen, the loop size be increased.

The resistivity values measured near the coast were very low (with a minimum of ~1 Ωm). Although electrical measurements from permafrost environments can show very high resistivity (e.g., Minsley et al., 2012), the values measured in our study are consistent with direct current electrical resistivity measurements collected from a saline permafrost environment in Barrow, Alaska, USA (Overduin et al., 2012) and previously in Adventdalen by Harada and Yoshikawa (1998), who observed a resistivity of 7.5Ωm at a depth of 30 m, and Ross et al (2007), who observed resistivities from ~10 to 400Ωm associated with two pingos (Hytte and Longyear Pingos). More recently, based on electrical resistivity imaging, Kasprzak et al. (2017) postulated the existence of unfrozen saline pore water near coastal zones in southern Svalbard. From our SNMR measurements we are able to confirm that such low resistivity values can indeed be attributed to the existence of unfrozen saline pore fluid.

The results from the SNMR and CSAMT data, showing unfrozen water content associated with low resistivity in substantial quantity and significant depths, are consistent with the sedimentological and cryospheric paleoenvironmental interpretations of the formation and evolution of permafrost in Adventdalen (Gilbert, 2018). Comparing the unfrozen water content detected by SNMR to laboratory measurements of the ice content in the 60 m CO_2 core from Adventdalen (location shown in Figure 1), which is in the range of 20 to 40% (Gilbert, 2014), we conclude that the permafrost in the lower Adventdalen is partially unfrozen. This assessment is consistent with the epigenetic origin of the permafrost, which developed after delta progradation down-valley filled Adventdalen with sediments following deglaciation since the early Holocene (Gilbert, 2018). Permafrost formation commenced and extended down-fjord through Adventdalen, when the fluvio-deltaic fjord-fill was subaerially exposed, and only the top syngenetic part of the permafrost below contained excess ice in a suite of cryofacies indicating ground-ice segregation and segregation intrusion (Gilbert, 2018). The lack of excess ice further down valley indicates that the source of moisture was limited to the saline pore water of the sedimentary deposits with no significant replenishment (Gilbert, 2018).

These results will also help predict permafrost degradation under the influence of ongoing climate warming in polar regions (Hansen et al., 2014; Isaksen et al., 2007). This is particularly important since unfrozen sediments can delay deep freezing, impact the sediment structure, permit groundwater upwelling to surface water bodies and/or may affect microbial activity thereby impacting greenhouse gas emissions (Grosse et al., 2011; Shur et al., 2005).

6 Conclusions

This study is the first to successfully map unfrozen water content in a coastal permafrost environment in the Arctic using SNMR and CSAMT. The SNMR measurements identified substantial unfrozen water content (up to ~10%) in the lower valley, near the coast in Adventdalen, Svalbard; the unfrozen water content decreased with distance from the coast as the age of the permafrost increased. No unfrozen water was detected above the upper marine limit. The CSAMT measurements supported the SNMR results. Low resistivities were observed in the lower valley; above the marine limit in the upper part of the valley, the resistivity was higher (>1000 Ωm in some locations).

The results of this study clearly demonstrate the utility of combining SNMR and CSAMT measurements to map the unfrozen water content in continuous permafrost. Combining the results presented here with thermal and geochemical data, including the pore water salinity, as well as the overall sedimentological and cryostratigraphical model for Adventdalen will allow development of a full assessment of the ice-content and thermal state of permafrost in

Adventdalen, Svalbard. Such a model is necessary to understand groundwater flow and its impact on periglacial features, such as pingos, and will allow us to quantify the potential release of greenhouse gasses.

Acknowledgements

The authors would like to thank Casey McGuffy and Sara Cohen for their support in the field. Funding for this research was provided by the Svalbard Science Forum and The University Centre in Svalbard. Travel support for Casey McGuffy was provided by the Rutgers Center for Global Advancement and International Affairs and the Newark Faculty of Arts and Sciences. We thank Mike Müller-Petke for discussions about MRSMATLAB. The geophysical data supporting this research is available through the Research Directory at Lancaster University (https://doi.org/10.17635/lancaster/researchdata/212). Permafrost thermal data from Adventdalen is available online through the NORPERM database at the Geological Survey of Norway (http://geo.ngu.no/kart/permafrost_svalbard/?lang=English).

References

Behroozmand, A., Keating, K., & Auken, E. (2015). A review of the principles and applications of the NMR technique for near-surface characterization. *Surveys in Geophysics*, *36*(1) 27-85. https://doi.org/10.1007/s10712-014-9304-0

Bense, V. F., Ferguson, G., and Kooi, H. (2009). Evolution of shallow groundwater flow systems in areas of degrading permafrost. *Geophysical Research Letters*, *36*, L22401. https://dio.org/10.1029/2009GL039225

Bense, V. F., Kooi, H. , Ferguson, G., and Read, T. (2012). Permafrost degradation as a control on hydrogeological regime shifts in a warming climate. *Journal of Geophysical Research, 117*, F03036. doi:10.1029/2011JF002143

Bobachev, C., (2002). IPI2Win: A windows software for an automatic interpretation of resistivity sounding data, Ph.D. thesis, Moscow State University.

Boike, J., Roth, K., & Overduin, P. P. (1998). Thermal and hydrologic dynamics of the active layer at a continuous permafrost site (Taymyr Peninsula, Siberia). *Water Resources Research, 34*(3), 355–363. https://doi.org/10.1029/97WR03498

Braun, M., & Yaramanci, U. (2008). Inversion of resistivity in magnetic resonance sounding. *Journal of Applied Geophysics*, *66*(3–4), 151–164. http://doi.org/10.1016/j.jappgeo.2007.12.004

Christiansen, H. H. (2005). Thermal regime of ice-wedge cracking in Adventdalen, Svalbard. *Permafrost and Periglacial Processes*, *16*, 87–98. https://doi.org/10.1002/ppp.523

Christiansen, H. H., Etzelmüller, B., Isaksen, K., Juliussen, H., Farbrot, H., Humlum, O., … Ødegård, R. S. (2010). The thermal state of permafrost in the Nordic area during the International Polar Year 2007-2009. *Permafrost and Periglacial Processes*, *21*, 156-181. https://doi.org/ 10.1002/ppp.68

French, H. M. (2007) *The Periglacial Environment*. Chichester, UK: John Wiley & Sons Ltd.

Gilbert, G. L. (2014). *Sedimentology and geocryology of an Arctic fjord head delta (Adventdalen, Svalbard)*, (Master's thesis). Oslo: University of Oslo & The University Centre in Svalbard.

Gilbert, G. L. (2018). *Cryostratigraphy and sedimentology of high-Arctic fjord-valleys*, (Ph.D Thesis). Longyearbyen: University of Bergen & University Centre in Svalbard.

Grombacher, D., Behroozmand, A. A., & Auken, E. (2017). Accounting for relaxation during pulse effects for long pulses and fast relaxation times in surface nuclear magnetic resonance. *Geophysics*, *82*(6), JM23-JM36. https://doi.org/10.1190/geo2016-0567.1

Grosse, G., Harden, J., Turetsky, M. McGuire, A. D., Camill, P., Tarnocai, C., … Striegl, R. G. (2011), Vulnerability of high-latitude soil organic carbon in North America to disturbance. *Journal of Geophysical Research*, *116*, G00K06. https://doi.org/10.1029/2010JG001507

Hansen, B. B., Isaksen, K. Benestad, R. E., Kohler, J., Pedersen, Å. Ø., Loe, L.E., … Varpe, Ø. (2014). Warmer and wetter winters: characteristics and implications of an extreme weather event in the High Arctic. *Environmental Research Letters*, *9*, 114021. https://doi.org /10.1088/1748-9326/9/11/114021

Harada, K., & Yoshikawa, K. (1998). Permafrost age and thickness at Moskuslagoon, Spitsbergen. *PERMAFROST – Seventh Internation Conference (Proceedings), Yellowknife, Canada*, *Collection Nordicana*, *55*, 427-431.

Hertrich, M. (2008). Imaging of groundwater with nuclear magnetic resonance. *Progress in Nuclear Magnetic Resonance Spectroscopy*, *53*, 227–248. https://doi.org/10.1016/j.pnmrs.2008.01.002

Hilbich, C., C. Hauck, M. Hoelzle, M. Scherler, L. Schudel, I. Völksch, D. Vonder Mühll, and R. Mäusbacher (2008), Monitoring mountain permafrost evolution using electrical resistivity tomography: A 7-year study of seasonal, annual, and long-term variations at Schilthorn, Swiss Alps, *Journal of Geophysical Research*, *113*, F01S90, doi:10.1029/2007JF000799

Hubbard, S. S., Gangodagamage, C., Dafflon, B., Wainwright, H., Peterson, J., Gusmeroli, A., … Wullschleger, S. D. (2013). Quantifying and relating land-surface and subsurface variability in permafrost environments using LiDAR and surface geophysical datasets. *Hydrogeology Journal*, *21*(1), 149–169. https://doi.org/10.1007/s10040-012-0939-y

Humlum, O. (2005). Holocene permafrost aggradation in Svalbard. In C. Harris, & J.B. Murton (Eds), *Cryospheric systems: Glaciers and Permafrost, Geological Society Special Publications*, (Vol. 242, pp. 119-130). Bath, UK: Geologic Society of London. https://doi.org/10.1144/GSL.SP.2005.242.01.11

Irons, T., Kass, M. A., & others, 2012, LemmaWeb, Lemma v1, https://lemmasoftware.org.

Isaksen, K., Sollid, J. L., Holmlund, P., & Harris, C. (2007). Recent warming of mountain permafrost in Svalbard and Scandinavia. *Journal of Geophysical Research*, *112*, F02S04. https://doi.org/10.1029/2006JF000522

Kasprzak, M., Strzelecki, M. C., Traczyk, A., Kondracka, M., Lim, M., & Migała, K. (2017). On the potential for a bottom active layer below coastal permafrost: the impact of seawater on permafrost degradation imaged by electrical resistivity tomography (Hornsund, SW Spitsbergen). *Geomorphology*, *293*, 347–359. https://dx.doi.org/10.1016/j.geomorph.2016.06.013

Kass, M. A., Irons, T. P., Minsley, B. J., Pastick, N. J., Brown, D. R. N., & Wylie, B. K. (2017). In situ nuclear magnetic resonance response of permafrost and active layer soil in boreal and tundra ecosystems. *The Cryosphere Discussion*. https://doi.org/10.5194/tc-2016-256

Kleinberg, R. L., & Griffin, D. D. (2005). NMR measurements of permafrost: unfrozen water assay, pore-scale distribution of ice, and hydraulic permeability of sediments. *Cold Regions Science and Technology*, *42*(1), 63–77. https://doi.org/10.1016/j.coldregions.2004.12.002

Koziar, A., & Strangway, D. W. (1978). Permafrost mapping by audiofrequency magnetotellurics. *Canadian Journal of Earth Sciences*, *15*(10), 1539–1545. https://doi.org/10.1139/e78-159

Lønne, I. (2005) Faint traces of high Arctic glaciations: an early Holocene ice-front fluctuation in Bolterdalen, Svalbard. *Boreas*, *34*, 308–323. http://dx.doi.org/10.1111/j.1502-3885.2005.tb01103.x

Lønne, I., & Nemec, W. (2004). High-Arctic fan delta recording deglaciation and environment disequilibrium. *Sedimentology*, *51*, 553-589. https://doi.org/10.1111/j.1365-3091.2004.00636.x

Mikucki, J. A., Auken, E., Tulaczyk, S., Virginia, R. A., Schamper, C., Sørensen, K. I., … Foley, N. (2015) Deep groundwater and potential subsurface habitats beneath an Antarctic dry valley. *Nature Communications*, *6*, 6831. https://doi.org/10.1038/ncomms7831

Minsley, B. J., Abraham, J. D., Smith, B. D., Cannia, J. C., Voss, C. I., Jorgenson, M. T., … Ager, T. A. (2012). Airborne electromagnetic imaging of discontinuous permafrost. *Geophysical Research Letters*, *39*(2), L02503. https://doi.org/10.1029/2011GL050079

Minsley, B. J., Pastick, N. J., Wylie, B. K., Brown, D. R. N, & Kass, A. M. (2016). Evidence for nonuniform permafrost degradation after fire in boreal landscapes. *Journal of Geophysical Research: Earth Surface*, *121*(2), 320-335. https://doi.org/10.1002/2015JF003781

Müller-Petke, M., Braun, M., Hertrich, M., Costabel, S.. & Walbrecker, J. (2016) MRSmatlab - A software tool for processing, modeling, and inversion of magnetic resonance sounding data. *Geophysics*, *81*, WB9-WB21. https://doi.org/10.1190/geo2015-0461.1

Müller-Petke, M., & Yaramanci, U. (2010). QT inversion—Comprehensive use of the complete surface NMR data set. *Geophysics*, *75*(4), WA199-WA209. https://doi.org/10.1190/1.3471523

NORPERM (Norwegian Permafrost Database) (2016). Online ground temperature data from Svalbard. http://www.tspnorway.com/ [accessed 7 December 2016]

Norsk Polarinstitutt. (2017). Online map data. http://toposvalbard.npolar.no/ [accessed 12 October 2017]

Overduin, P. P., Westermann, S., Yoshikawa, K., Haberlau, T., Romanovsky, V., & Wetterich, S. (2012). Geoelectric observations of the degradation of nearshore submarine permafrost at Barrow (Alaskan Beaufort Sea). *Journal of Geophysical Research: Earth Surface*, *117*, F02004. https://doi.org/10.1029/2011JF002088

Parsekian, A. D., Grosse, G., Walbrecker, J. O., Müller-Petke, M., Keating, K., Liu, L., … Knight, R. (2013). Detecting unfrozen sediments below thermokarst lakes with surface nuclear magnetic resonance. *Geophysical Research Letters*, *40*(3), 1–6. https://doi.org/10.1002/grl.50137

Romanovsky, V. E., & Osterkamp, T. E. (2000). Effects of unfrozen water on heat and mass transport processes in the active layer and permafrost. *Permafrost and Periglacial Processes*, *11*(3), 219-239. https://doi.org/10.1002/1099-1530(200007/09)11:3<219::AID-PPP352>3.0.CO;2-7

Ross, N., Brabham, P. J., Harris, C., & Christiansen, H. H. (2007). Internal structure of open system pingos, Adventdalen, Svalbard: the use of resistivity tomography to assess ground-ice conditions. *Journal of Environmental & Engineering Geoscience*, *12*(1), 113-126. https://doi.org/10.2113/JEEG12.1.113

Shur, Y., Hinkel, K. M., & Nelson, F. E. (2005). The transient layer: Implications for geocryology and climate-change science. *Permafrost Periglacial Process*es, *16*(1), 5–17. https://doi.org/10.1002/ppp.518

Walbrecker, J. O., Hertrich, M., & Green, A. G. (2009). Accounting for relaxation processes during the pulse in surface NMR data. *Geophysics*, *74*(6), G27–G34. https://doi.org/10.1190/1.3238366

Walbrecker, J. O., Hertrich, M., & Green, A. G. (2011) Off-resonance effects in surface nuclear magnetic resonance. *Geophysics*, *77*(2), G1-12. https://doi.org/10.1190/1.3535414

Walsh, D. O. (2008). Multi-channel surface NMR instrumentation and software for 1D/2D groundwater investigations. *Journal of Applied Geophysics*, *66*(3-4), 140–150. https://doi.org/10.1016/j.jappgeo.2008.03.006

Walvoord, M. A., & Kurylyk, B. L. (2016). Hydrologic impacts of thawing permafrost—A review. *Vadose Zone Journal*, *15*(6), vzj2016.01.0010. https://doi.org/10.2136/vzj2016.01.0010

Figure Captions

Figure 1: Terrain model of the Adventdalen valley showing the locations of the CSAMT and SNMR measurements. The road is shown as a light brown line. The model is from the Norwegian Polar Institute; http://toposvalbard.npolar.no (Norsk Polarinstitutt, 2017). The inset is from Google Earth.

Figure 2: Annual ground thermal conditions in the permafrost in the Adventdalen valley. Data are from the valley bottom borehole AS-B2 for the hydrological year 1 September 2012 to 31 August 2013. The black lines show the maximum and minimum average daily temperature during this year; the red lines show the maximum and minimum average daily temperature during the study period 23 March to 2 April 2013; the horizontal line denotes the interpolated depth of the active layer (NORPERM, 2016).

Figure 3: Inverted SNMR and CSAMT depth profiles of unfrozen water content and resistivity for the down-valley profile (locations as shown in Figure 1) for data collected in Adventdalen, Svalbard. Horizontal red lines indicate the approximate depth of investigation of the SNMR measurements. Labels above the profiles indicate which CSAMT measurement was used in the inversion of the SNMR data, but only collocated or independent CSAMT measurements are shown. The thin grey lines on the SNMR profiles indicate the uncertainty in the inversion and are models that fit the data approximately as well as the model of best fit (thick blue line). The spacing between the measurements made in the upper-valley indicates that these measurements were made further apart (not to scale).

Figure 4: Inverted SNMR and CSAMT depth profiles of unfrozen water content and resistivity for the across-valley profiles (locations as shown in Figure 1) collected in Adventdalen,

Svalbard. Horizontal red lines indicate the approximate depth of investigation of the SNMR measurements. Labels above the profiles indicate which CSAMT measurement was used in the inversion of the SNMR data, but only collocated CSAMT measurements are shown. The thin grey lines on the SNMR profiles indicate the uncertainty in the inversion and are models that fit the data approximately as well as the model of best fit (thick blue line).

Figure 1.

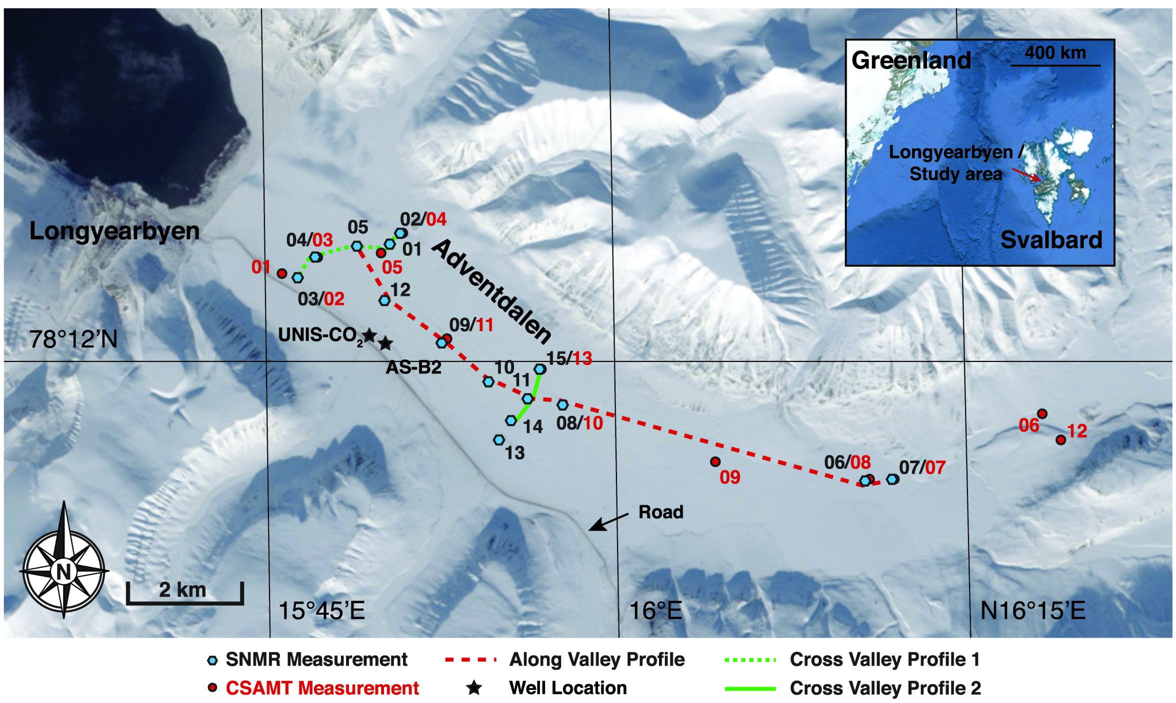

Greenland
400 km
Longyearbyen / Study area
Svalbard
Longyearbyen
Adventdalen
78°12'N
UNIS-CO2
AS-B2
Road
2 km
15°45'E
16°E
N16°15'E
01
04/03
05
02/04
01
05
03/02
12
09/11
10
11
15/13
14
08/10
13
09
06/08
07/07
06
12
SNMR Measurement
CSAMT Measurement
Along Valley Profile
Well Location
Cross Valley Profile 1
Cross Valley Profile 2

Figure 2.

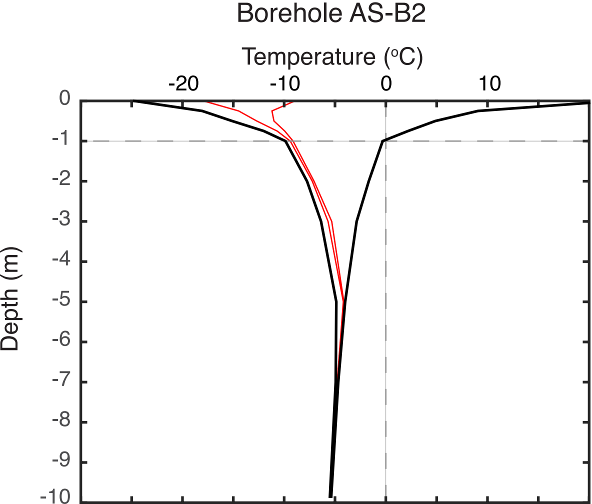

Borehole AS-B2
Temperature (°C)
-20
-10
0
10
0
-1
-2
-3
-4
-5
-6
-7
-8
-9
-10
Depth (m)

Figure 3.

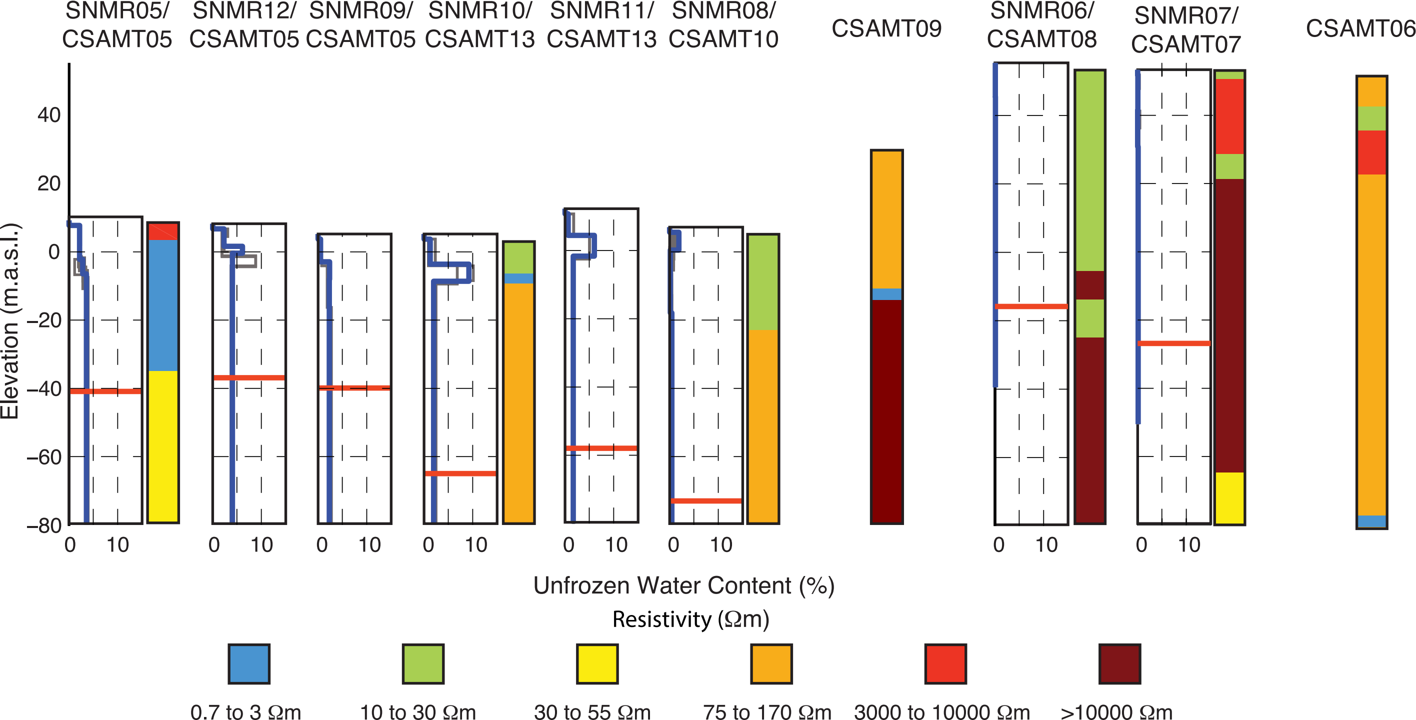

SNMR05/ CSAMT05
SNMR12/ CSAMT05
SNMR09/ CSAMT05
SNMR10/ CSAMT13
SNMR11/ CSAMT13
SNMR08/ CSAMT10
CSAMT09
SNMR06/ CSAMT08
SNMR07/ CSAMT07
CSAMT06
Elevation (m.a.s.l.)
40
20
0
−20
−40
−60
−80
0
10
Unfrozen Water Content (%)
Resistivity (Ωm)
0.7 to 3 Ωm
10 to 30 Ωm
30 to 55 Ωm
75 to 170 Ωm
3000 to 10000 Ωm
>10000 Ωm

Figure 4.

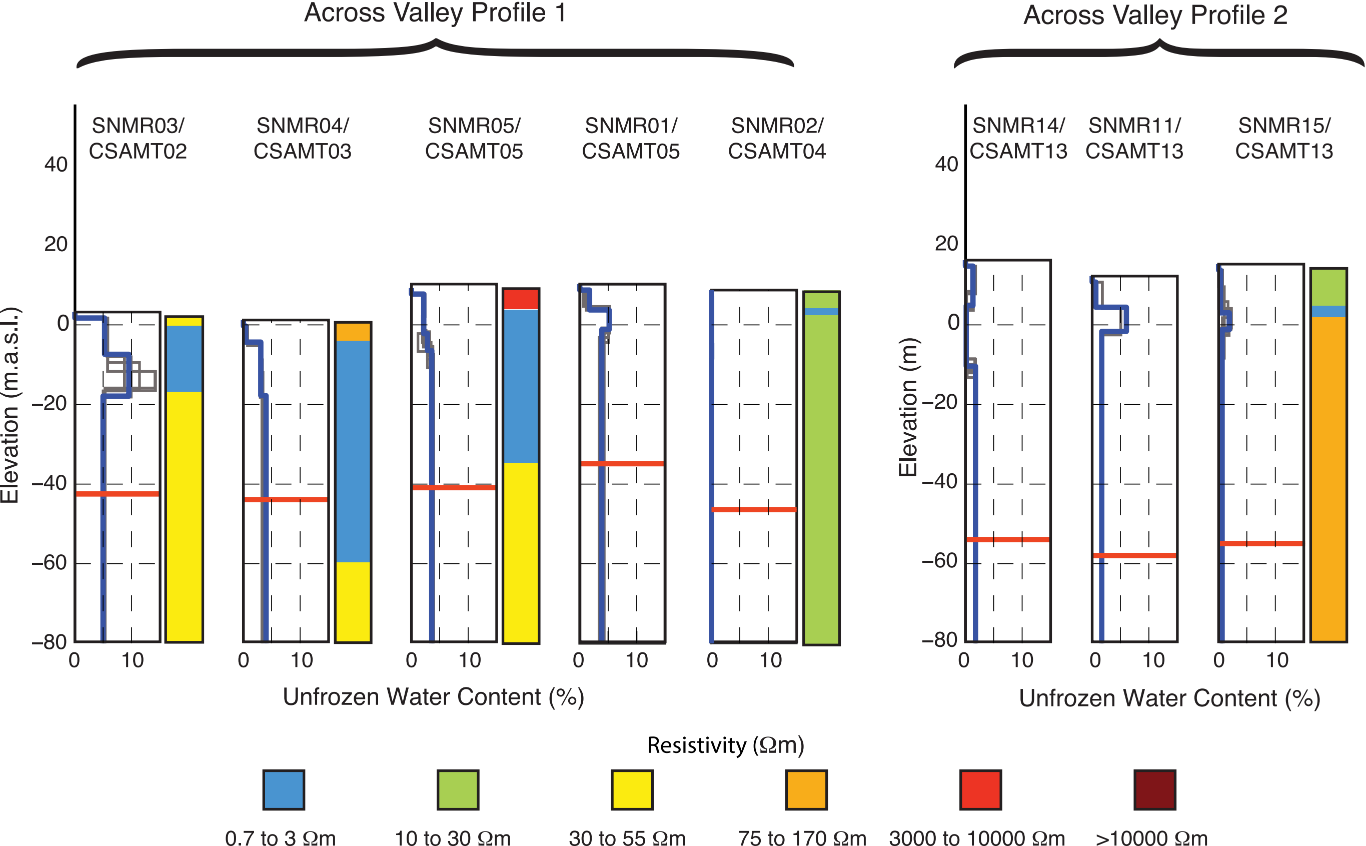

Across Valley Profile 1
Across Valley Profile 2
SNMR03/
CSAMT02
SNMR04/
CSAMT03
SNMR05/
CSAMT05
SNMR01/
CSAMT05
SNMR02/
CSAMT04
SNMR14/
CSAMT13
SNMR11/
CSAMT13
SNMR15/
CSAMT13
Elevation (m.a.s.l.)
Elevation (m)
40
20
0
−20
−40
−60
−80
0
10
Unfrozen Water Content (%)
Unfrozen Water Content (%)
Resistivity (Ωm)
0.7 to 3 Ωm
10 to 30 Ωm
30 to 55 Ωm
75 to 170 Ωm
3000 to 10000 Ωm
>10000 Ωm